Blocking and Westward Passage of Eddies in the Luzon Strait

Woei-Jen Sheu [a], Chau-Ron Wu [a,b,*], Lie-Yauw Oey [b]

[a] Department of Earth Sciences, National Taiwan Normal University, Taipei, Taiwan
[b] Program in Atmospheric and Oceanic Sciences, Princeton University, Princeton, USA

ARTICLE INFO

ABSTRACT

Satellite observations have shown the abundance of generally westward-propagating eddies in the subtropical regions in the North Pacific Ocean, especially north of 10°N. Eddies transport mass, and can significantly impact the circulation as well as the heat, salt and nutrient balances of the western Pacific marginal seas. This paper uses a numerical model to examine the conditions when eddies can or cannot freely propagate westward through the Luzon Strait into the South China Sea (SCS). Composite analyses on the 10-year model data show that the fates of eddies depend on the strength and path of the Kuroshio. In one path that exists mostly during fall and winter, the Kuroshio loops westward into the SCS, the potential vorticity (PV) across the current is weak, and eddies are likely to propagate freely through the Luzon Strait. In another path, which exists mostly during spring and summer, the Kuroshio tends to leap directly northward bypassing the SCS, the PV across it strengthens, and eddies are then blocked and are constrained to also follow the northward path. Nonlinear eddy-current interaction and the existence of a cyclone north of the Luzon Island during the looping phase explain why eddies of both signs can pass through the strait. It is shown also that the upstream state of the Kuroshio in the western tropical Pacific plays an important role in dictating the different paths of the Kuroshio. The looping (leaping) path is caused by a weakened (stronger) Kuroshio transport related to the northward (southward) shift of the North Equatorial Current in wintertime (summertime).

© 2010 Elsevier Ltd. All rights reserved.

1. Introduction

The subtropical North Pacific contains a large number of eddies produced most likely by instabilities in the long baroclinic Rossby waves (LaCasce and Pedlosky, 2004). The propagation of eddies are related to the phase speeds of Rossby waves (Roemmich and Gilson, 2001; Chelton et al., 2007). Hwang et al. (2004) used TOPEX/Poseidon altimeter data to show that the averaged speed of the westward-moving mesoscale eddies (both warm-core and cold-core) near 22°N is approximately 8 km/day (~9 cm/s) and the propagation direction can be altered when eddies encounter topography or when they interact with other eddies. Eddies transport mass, and can therefore significantly impact the circulation as well as the heat and salt balances of the western Pacific marginal seas.

The westward propagating eddies reach the western North Pacific where they interact with the Kuroshio, and may modulate the Kuroshio transport and path (Yang et al., 1999; Zhang et al., 2001; Yuan et al., 2006). In the present study, we focus on the fate of eddies as they interact with the Kuroshio east of the Luzon

Strait. The Luzon Strait is a gap in the western boundary. The northward-flowing Kuroshio sometimes loops or intrudes into the South China Sea through the Luzon Strait before continuing northward along the east coast of Taiwan (Shaw, 1991; Wu and Chiang, 2007). The seasonal, intra-seasonal and interannual variability of the Kuroshio intrusion has been reported from various observations (e.g., Centurioni et al., 2004; Ho et al., 2004; Liang et al., 2008) and model simulations (Farris and Wimbush, 1996; Wu and Chiang, 2007; Hsin et al., 2008). Between 1989–2002 drifters were tracked to enter the South China Sea between October and December (Centurioni et al., 2004). Wu and Chiang (2007) also found that the westward intrusion (i.e. looping) of the Kuroshio through the Luzon Strait in December is more often than in August. In summer, the Kuroshio would tend to "leap" across the Luzon Strait without making a westward loop. The seasonal variability of Kuroshio looping or leaping (we follow Sheremet (2001) in using the terms "looping" and "leaping" to describe the two modes of Kuroshio in the Luzon Strait) is likely to depend on the strength of transport, which can in turn affects how eddies behave when they propagate near the Kuroshio. In this paper, we examine if eddies can cross the Kuroshio and propagate westward through the Luzon Strait. A nested three-dimensional, primitive-equation numerical ocean model is implemented to gain an understanding of the interplay between the strong boundary current and eddies. Model results over the Philippine Sea and the South China Sea are analyzed to describe the eddy movements. We show that eddies can more

* Corresponding author at: Department of Earth Sciences, National Taiwan Normal University, 88, Section 4 Ting-Chou Road, Taipei 11677, Taiwan.
Tel.: +886 229329042; fax: +886 229333315.
E-mail address: cwu@ntnu.edu.tw (C.-R. Wu).

easily cross the Kuroshio and intrude into the South China Sea in fall-winter, and that in other seasons they tend to be carried northward across the Luzon Strait by the Kuroshio. We find that these distinct characteristics are a function of the two modes of the Kuroshio – looping and leaping – which in turn are a function of the upstream state of the Kuroshio. In particular, we will show that the Kuroshio transport and potential vorticity (PV) distribution depend on the meridional shift in the North Equatorial Current (NEC). Northward shift of NEC in fall and winter weaken both the transport and the PV-gradient across the Kuroshio, allowing westward-propagating eddies from the Pacific to more readily intrude into the South China Sea.

2. The Model

The model is based on the Princeton Ocean Model (POM); it is called EAMS (East Asian Marginal Sea; Wu and Hsin, 2005). The three-dimensional, free surface model solves the primitive equations for momentum, salt and heat. It includes a 2.5-level turbulence closure sub-model developed by Mellor and Yamada (1974, 1982) and the Smagorinsky formulation for horizontal mixing (Smagorinsky, 1963). Additional information on the POM can be found in Mellor (2004). The EAMS model spans the region from 99°E to 140°E in longitude and from 0°N to 42°N in latitude (Fig. 1). The horizontal grid resolution is 1/8° (about 13.5 km), and there are 26 sigma levels in the vertical. At the open boundaries, the EAMS model derives its boundary condition from a larger-scale North Pacific Ocean (NPO; Hsin et al., 2008) model, from 16°S to 60°N latitude and 99°E to 77°W longitude.

During spin-up, the EAMS model is initialized by the temperature and salinity fields of the NPO model output in January 1980 and then integrated using climatological forcing through 1992. The EAMS model is then forced by the six-hourly NCEP/NCAR reanalysis version 2 wind stress at the sea surface. The simulation period is from 1993 to 2002. The EAMS model has been validated against hydrographic data in the South China Sea (Tseng et al., 2005), as well as against the Acoustic Doppler Current Profiler (ADCP) observations in the Taiwan Strait (Wu and

Hsin, 2005) and also in the Kuroshio east of Taiwan (Hsin et al., 2008). As will be seen below, the model also simulates the Kuroshio and westward propagating eddies in the Pacific Ocean, similar to those observed in the satellite observations (Hsin et al., 2008). The model therefore provides a dynamically self-consistent simulation that we can analyze to extract physical processes relating to the Kuroshio and eddy interactions.

3. The Jet-Eddy Interaction Problem

The problem of jet-eddy interaction has been considered by various authors. It is instructive to review here Vandermeirsch et al. (2003a) who describe the essential dynamics based on the reduced-gravity model. Vandermeirsch et al. (2003b) also extend the calculations to a two-layer system but the essential elements of the reduced-gravity model remain unchanged.

Consider an eddy, either cyclonic or anticyclonic, drifting westward and approaching a straight meridional jet (Fig. 2A). The jet's velocity is a maximum along its center ($x=0$), and exponentially decays symmetrically on either side. Such a velocity profile is obtained by specifying a constant potential vorticity (PV) jump across the jet:

$$PV_{Jet} = +\Delta Q_J/2, x > 0,$$
$$= -\Delta Q_J/2, x < 0,$$

so that $PV\text{-jump}|_{Jet} = \Delta Q_J$. Similarly, for the eddy, assumed to be of a circular shape with radius R_{Eddy}, we have,

$$PV_{Eddy} = \Delta Q_E, \quad r < R_{Eddy},$$
$$= 0, \quad r < R_{Eddy},$$

and the $PV\text{-jump}|_{Eddy} = \Delta Q_E$. Here, r denotes the radial distance from the center of the eddy.

For a weak eddy and/or a strong jet, such that $\Delta Q_J > \Delta Q_E$ (Fig. 2B), the mutual interaction between eddy and jet is small; the eddy does not cross the jet and is being advected along with the jet [Stern and Flierl, 1987; Bell, 1990]. If the eddy's strength is increased and/or the jet's strength is weakened, $\Delta Q_E > \alpha\Delta Q_J$, where $\alpha > 1$, the eddy interacts nonlinearly with the jet. The
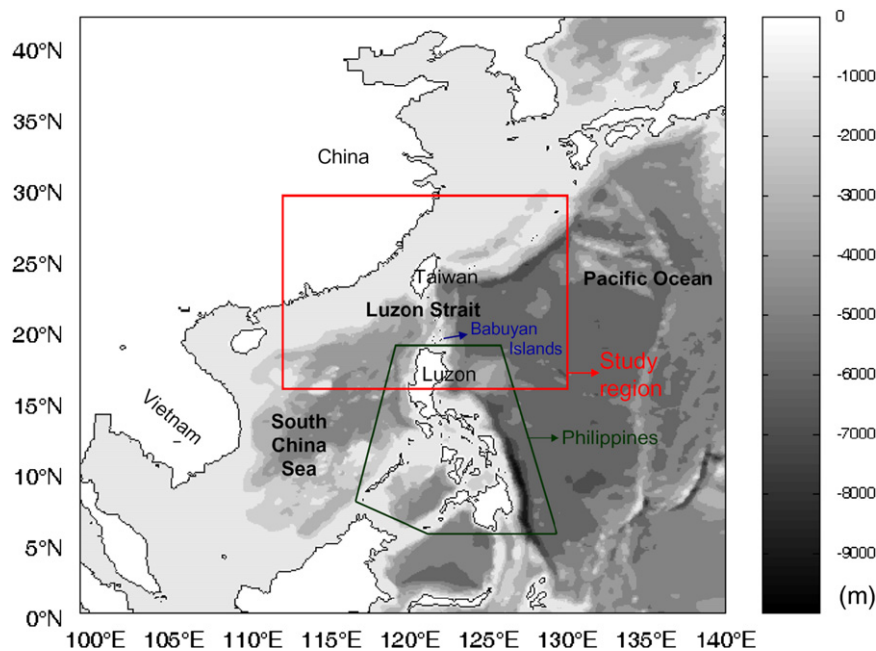

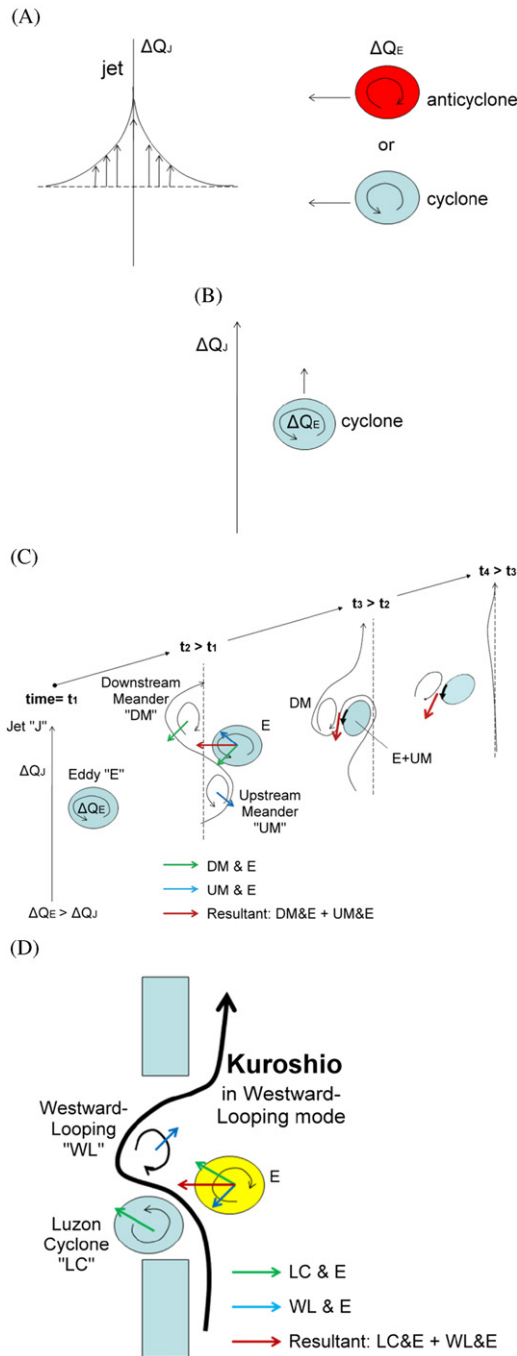Fig. 1. The East Asian Marginal Seas (EAMS) model domain and bathymetry.

Fig. 2. A sketch of (A) the jet with PV-jump$|_{Jet}=\Delta Q_J$, and the approaching eddy with PV-jump$|_{Eddy}=\Delta Q_E$, (B) a weak (cyclonic) eddy and/or a strong jet, $\Delta Q_J > \Delta Q_E$; the eddy does not cross the jet but is advected along with the jet; (C) the evolution at four indicated times for the combined system of a strong (cyclonic) eddy and/or a weak jet, $\Delta Q_E > \Delta Q_J$; and (D) anticyclone "E" interacting with the westward-looping mode of the Kuroshio with embedded Luzon Cyclone "LC" and the Westward-Looping meander "WL".

eddy's velocity field can then significantly influence the jet, and the jet's velocity field in turn affects the eddy. The evolution of the combined system of a cyclone and jet is illustrated in Fig. 2C at four time instances, $t_1 < t_2 < t_3 < t_4$. Time t_1 is when the jet begins to "feel" the presence of the eddy "E," when the latter comes within $2R_o$ of the jet's axis, where R_o is the Rossby radius. The sketch at time $=t_2$ shows that the eddy's velocity field down-stream (upstream) shifts the jet westward (eastward) to develop the downstream (upstream) meander "DM" ("UM"). Vorticity

inside "DM" ("UM") is anticyclonic (cyclonic). The "dipole" formed by DM and E moves southwestward due to their mutually induced velocity shown by the green vector, while UM and E also have a mutually-induced velocity shown by the blue vector. The resultant vector is westward indicated by the red vector in a direction that tends to cross the jet. Fig. 2C shows how this jet-crossing may occur at a later time $=t_3$, during which the E and UM merge, but the DM-E dipole continues to "peal" itself from the jet. This "pealing" process is complete at time $=t_4$ when the original eddy E has completely crossed the jet.

If eddy "E" is an anticyclone, then the same argument will show that the eddy cannot cross the jet (the resultant (red; Fig. 2C) vector would be eastward). However, the above considers only a straight jet. In the case of the Kuroshio in the Luzon Strait, our numerical simulation will show that in the "looping" mode, a cyclone develops north of the Luzon Island just as the Kuroshio loops westward into the South China Sea; this westward-looping mode of the Kuroshio is sketched in Fig. 2D. The cyclone will be called the "Luzon Cyclone" and we will later discuss its origin. Fig. 2D also shows an anticyclone approaching the Kuroshio, and it is clear that westward crossing is now possible; the same reasoning applies equally to an approaching cyclone. As in Vandermeirsch et al. (2003a), the eddy's and jet's strengths, ΔQ_E and ΔQ_J, will again dictate if jet-crossing occurs.

The above suggests that the relative strengths of the Kuroshio (i.e. the jet; ΔQ_J) and eddy (ΔQ_E), as well as whether or not the Kuroshio is in a leaping or looping mode, dictate if an eddy from the Pacific would intrude westward through the Luzon Strait when it interacts with the Kuroshio. When the Kuroshio is in the leaping mode, a strong cyclone may intrude into the South China Sea. When the Kuroshio is in the looping mode, eddies of both signs can cross the current. Moreover, we will show that the leaping (looping) mode is characterized by strong (weak) transport, as well as large (small) PV-jump across the Kuroshio. Therefore, we expect westward passage of eddies to occur most frequently during fall-winter season when the Kuroshio is in its looping mode.

4. Propagating Eddies

We demonstrate the existence of propagating eddies in the model, first by way of the Empirical Orthogonal Function (EOF; e.g., Lorenz, 1956) and Complex Empirical Orthogonal Function (CEOF; e.g., Horel, 1984) analyses, then through a composite EOF-analysis technique commonly used to analyze climate data.

4.1. EOF analysis

To study eddy propagation, we performed the EOF analysis on the sea surface height anomaly (SSHA) obtained by first removing the annual signal from the 10-year model output. The study region is from 112°E to 128°E and 15°N to 28°N. EOF decomposition of SSHA yields two dominant modes, explaining 27% and 24% of the variance, respectively. Fig. 3A shows the spatial distribution of EOF-mode 1, which shows the counter-rotating eddy pair centered at 127°E, 17°N and 124°E, 17°N. Another single eddy is located east of Taiwan, centered at 123°E, 22°N. The time series of EOF-mode 1 is shown in Fig. 3B. The time series of EOF-mode 1 shows intra-seasonal variability, and the period is approximately 70 days.

The spatial distribution of EOF-mode 2 is shown in Fig. 4A. Similar to the spatial pattern of mode 1, there is a pair of counter-rotating eddies off the northeastern Luzon, although the location of the maximum amplitude oscillations is slightly to the west, centered at 126°E, 16°N and 123°E, 17°N. The eddy centered at
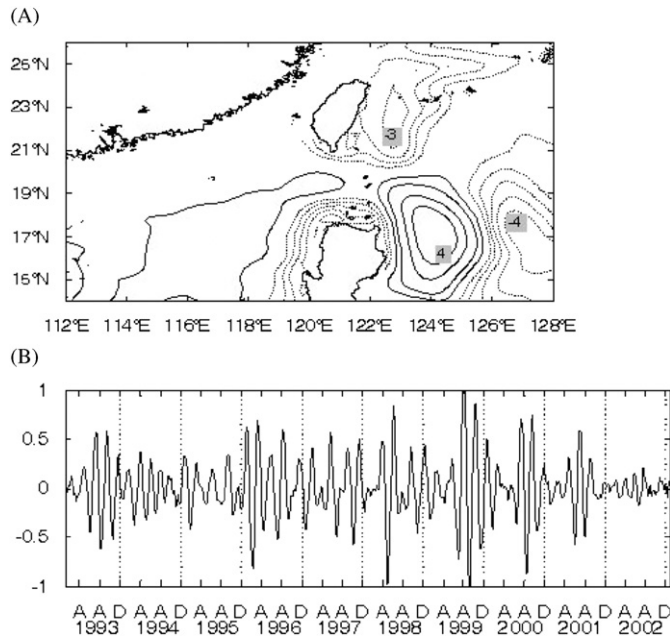
(A)

(B)

Fig. 3. EOF analysis of the mode-1 of modeled SSHA fields. The contour interval is 1 cm. (A) spatial distribution and (B) time series variability.
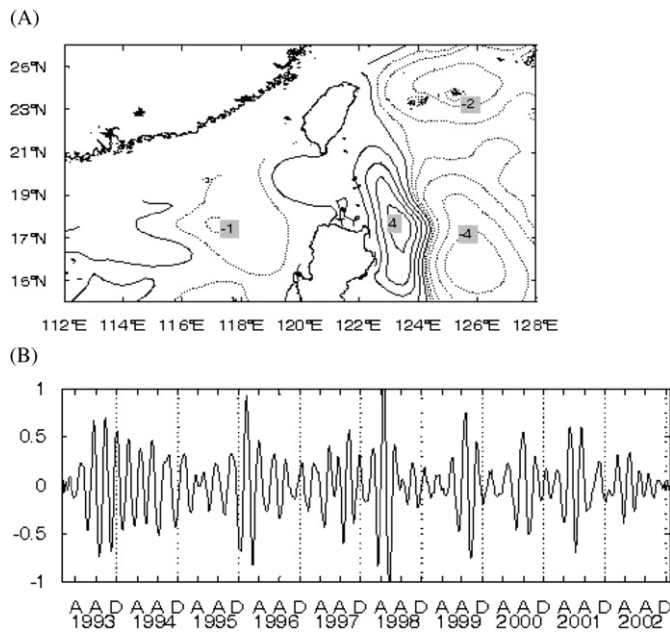
(A)

(B)

Fig. 4. Same as Fig. 3 but for the mode-2: (A) spatial distribution and (B) time series variability.

123°E, 17°N is elongated in the meridional direction as the eddy encounters the land boundaries. There is also a pair of weak eddies in the northeastern South China Sea, centered at 118°E, 17°N and 114°E, 17°N. The single eddy east of Taiwan in Fig. 3A migrates toward the northeastern Taiwan as shown in Fig. 4A. The spatial distribution of EOF-mode 2 shown here seems to be a propagating mode of that of EOF-mode 1. The time series of EOF-mode 2 (Fig. 4B) corresponds well to that of EOF-mode 1 (Fig. 3B), and both of them display a similar intra-seasonal variability. The temporal pattern of EOF-mode 1 leads that of EOF-mode 2 by 3 weeks with a high correlation coefficient of 0.6 (figure not shown). Fig. 5 shows the spectral analysis of EOF-mode 1 and
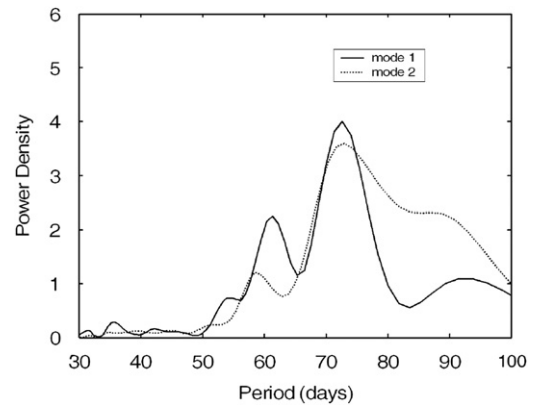

Fig. 5. Spectral analysis of EOF-mode 1 and EOF-mode 2.

EOF-mode 2. The spectrum for EOF-mode 1 has a major peak at 72-days and a minor peak at 60-day, while the spectrum for EOF-mode 2 also has a major peak at 72-days and a minor peak at 58-day.

4.2. CEOF analysis

A frequency domain, CEOF is used to further determine the eddy evolution and propagation. Fig. 6A shows the spatial amplitude distribution of CEOF-mode 1 (variance=34%). A train of large-amplitude eddies are seen on both sides of the Luzon Strait. Fig. 6B shows the temporal amplitude distribution. The fluctuation frequency of CEOF-mode 1 is around 60–70 days. The amplitude for the year 1998 is much higher than the other years in the study period, caused by an exceptionally strong La Niña event. Fig. 6C shows the spatial amplitude distribution of CEOF-mode 2 (variance=30%). Large amplitude eddies centered at 126°E, 15°N and 124°E, 17°N off the eastern Luzon Island are observed. A weak amplitude eddy centered at 125.5°E, 24°N is also displayed. Fig. 6D shows that the time series of amplitude has a period of 70 days, in agreement with the intra-seasonal variability shown in EOF-mode 2.

Fig. 7A shows the spatial distribution of phase for CEOF-mode 1. The phase propagates from the eastern side off the Luzon Island toward the South China Sea as well as from southeastern Taiwan toward northeastern Taiwan. Fig. 7B shows the phase time series for CEOF-mode 1 and shows a period of 60–70 days. Fig. 7C shows the spatial distribution of phase for CEOF-mode 2. Away from the eastern side of Luzon Island, the phase is propagating from the east to the west. Inside the Luzon Strait, the phase propagates northward. In Fig. 7D, the time series of CEOF-mode 2 shows intra-seasonal variability with a period of 60–70 days. The period and propagation speed of eddies are in a good agreement with those estimated by the Satellite altimeter data (figure not shown). In summary, CEOF-mode 1 mainly represents westward eddy-propagation through the Luzon Strait into the South China Sea, and CEOF-mode 2 represents northward propagation of eddies; these latter eddies migrated westward from the Pacific Ocean but are blocked east of the Luzon Strait.

4.3. Temperature structure

Fig. 8 shows the longitude-time contours of the modeled temperature anomalies at a depth of 65 m along 19°N. The anomalies are computed by removing an annual running mean. Westward-propagating features are clearly seen and the estimated speed is about 8–9 km/day (9–10.5 cm/s), which is
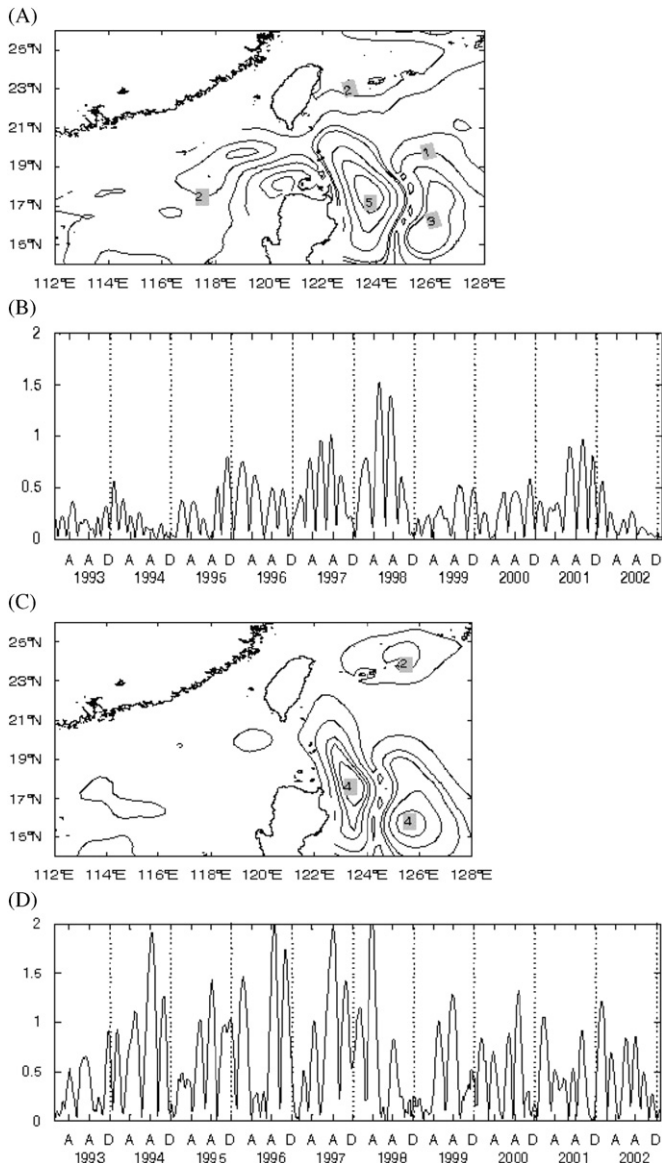
Fig. 6. CEOF analysis of the mode-1 amplitude for the modeled SSHA fields: (A) spatial distribution and (B) temporal distribution. The results of CEOF mode-2 amplitude fields: (C) spatial distribution and (D) temporal distribution.
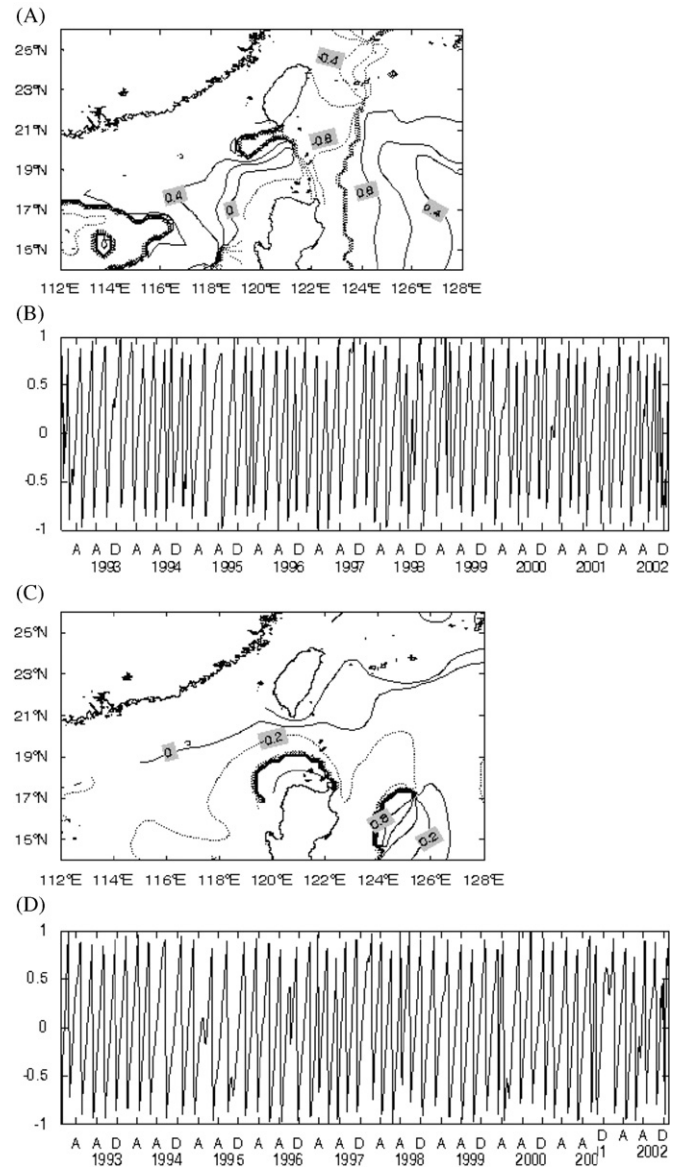

Fig. 7. Same as Fig. 6 but for the phase fields: (A) CEOF mode-1 spatial distribution, (B) CEOF mode-1 temporal distribution, (C) CEOF mode-2 spatial distribution, and (D) CEOF mode-2 temporal distribution.

consistent with the phase speed of the first baroclinic mode Rossby Wave estimated by Chelton and Schlax (1996). Composite analysis (e.g. Knutson and Weickmann, 1987) with daily temperature is applied to examine the evolution of the model eddies. Let $\overline{T}(X_i, Z_i) = 1/n \sum_{t=1}^{n} T(X_i, Z_i, t)$ and the present time t_0 is composited by the positive peak eigenvalues of EOF-mode 1. The time sequence denotes $t_{-1} = t_0 - 1$ week and $t_1 = t_0 + 1$ week at 1-week interval. The de-trended temperature data are normalized by the maximum temperature. Fig. 9 shows the evolution of the vertical temperature structure at depths from 50 to 350 m along 19°N at a regular interval of one week. The eddy structure is well developed until eddy encounters the sharp terrain near Babuyan Islands, which makes eddy's structure diffuse and incoherent. In the meridional direction, vertical temperature structure along 124°E (Fig. 10) shows that eddies propagate northward at an average speed of 1° latitude/week ($\sim$18 cm/s), which is approximately two times faster than the speed of westward-propagating eddies. Both warm and cold eddies are seen and the maximum variation in the temperature core occurs at 100 m and

extends down to a depth of 200 m. As eddies pass the latitudes 21°N to 22°N, the temperature shows less coherent vertical structures caused by a tendency for the Kuroshio to develop a meander near the mid-section of the Luzon Strait (see also Figs. 11 and 12 below).

5. Blocking and Westward Passage of Eddies in the Luzon Strait

The above analyses indicate the existence of two dominant modes describing the fates of westward-propagating eddies as they approach the Luzon Strait. In one mode, the eddy passes through the Strait. In the other mode, the eddy follows the northward-flowing Kuroshio towards the east coast of Taiwan. In this section, we relate these two modes to the different states of the Kuroshio. We composite the 10-year circulation patterns in the upper layer (0–150 m) into (i) the westward-passage pattern Ew and (ii) the blocking or northward-propagating pattern En. We then
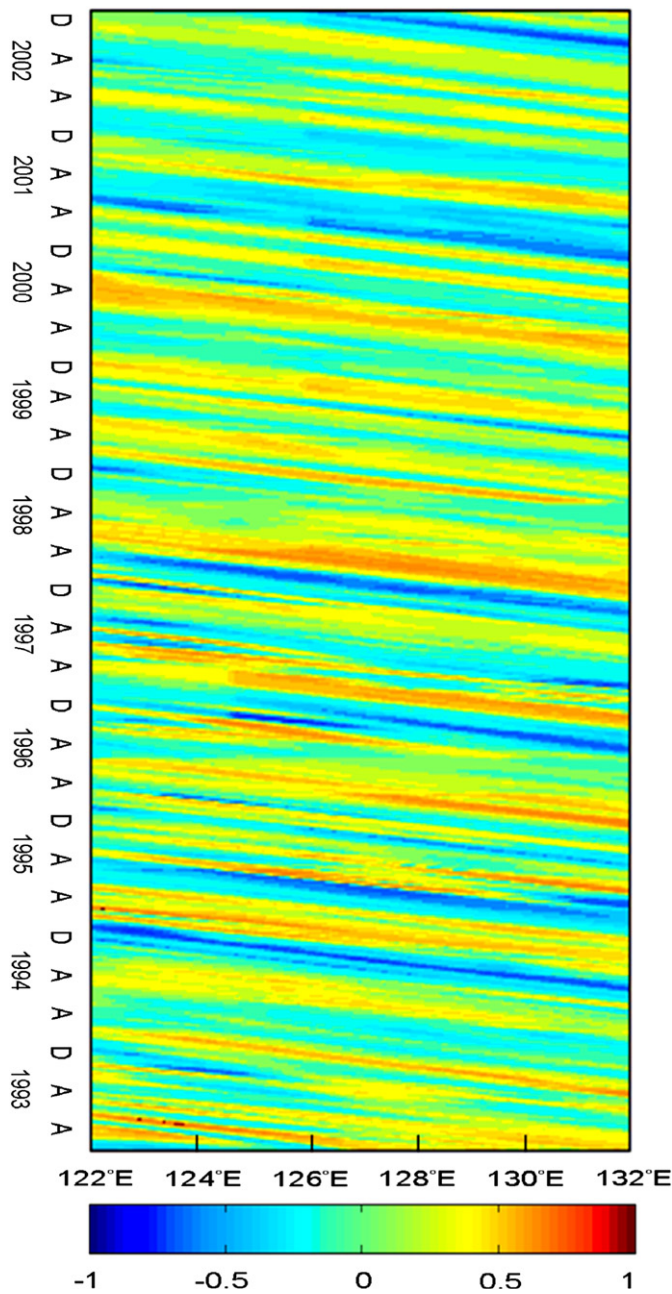
Fig. 8. The time-longitude diagram of modeled temperature anomalies at 65 m along 19°N (Blue represents negative and red is positive).

ensemble-average them into $\overline{Ew}$ and $\overline{En}$, respectively. The $\overline{Ew}$ ensemble consists of maps that are predominantly for fall and winter while the $\overline{En}$ ensemble is from the spring and summer maps.

Figs. 11 and 12 show the ensemble-averaged composites $\overline{Ew}$ and $\overline{En}$, respectively. Though westward propagation of eddies of both signs exist, we show in Figs. 11 and 12 only the "warm" or anticyclonic eddy case. Vectors show the current, and the color shading represents the vorticity (unit: 10^{-5}/s). Here, anticyclonic vorticity is red indicating generally warmer waters and cyclonic vorticity is blue indicating generally cooler waters. Panels (a) of both Figures (Figs. 11A and 12A) show the composite patterns at the times of analysis when an eddy first interacts with the Kuroshio east of the Luzon Strait. The beginning of the interaction is defined as when an eddy is near 124°E, 19°N.

Fig. 11 shows westward passage of eddies through the Luzon Strait, while in Fig. 12 eddies are blocked and propagate northward directly along the eastern flank of the Kuroshio from Luzon to Taiwan. Comparing these figures, it is clear that the westward-passage pattern ($\overline{Ew}$) is concomitant with a northward shift in the bifurcation of the NEC, around 14–15°N in fall-winter (Fig. 11), from its location during the blocking pattern $\overline{En}$ in spring-summer, when the bifurcation is further south at 11–12°N (Fig. 12). The seasonal shifts of the bifurcation location agree with those inferred from hydrographic data (Qu and Lukas, 2003), and also from satellite measurements (Wang and Hu, 2006). The (modeled) NEC bifurcation latitude is also related to the Kuroshio transport; this is shown in Fig. 13, which shows strong (weak) transport in spring-summer (fall-winter) when the bifurcation latitude shifts south (north). It is clear that the blocking ($\overline{En}$) pattern coincides with the period when the Kuroshio is more intense, with transport ≈ 30–35 Sv, and that the transport is weaker, about 18–22 Sv, during the westward-passage pattern ($\overline{Ew}$).

One expects then that the stronger inertia during the blocking pattern would enable the Kuroshio to more readily 'leap' across the Luzon Strait, while during the weakened transport of the westward-passage pattern the Kuroshio would tend to 'loop' westward into the South China Sea through the Strait. Such 'leaping' and 'looping' scenarios of a western boundary current and their dependence on the inertia have been nicely illustrated in a reduced-gravity model by (Sheremet, 2001; a laboratory experimental confirmation of the phenomenon is given in Sheremet and Kuehl, 2007). In his model, the looping (or "penetrating") scenario generally occurs at low Reynolds numbers and a cyclone is produced south of the Loop (e.g. see Sheremet's Fig. 6A). The comparison between Sheremet's model with our 3-D model with continuous stratification is not exact, but one can see in Fig. 11A the occurrence also of a cyclone (vorticity $> 0.6 \times 10^{-5}$/s) north of the Luzon Island during the
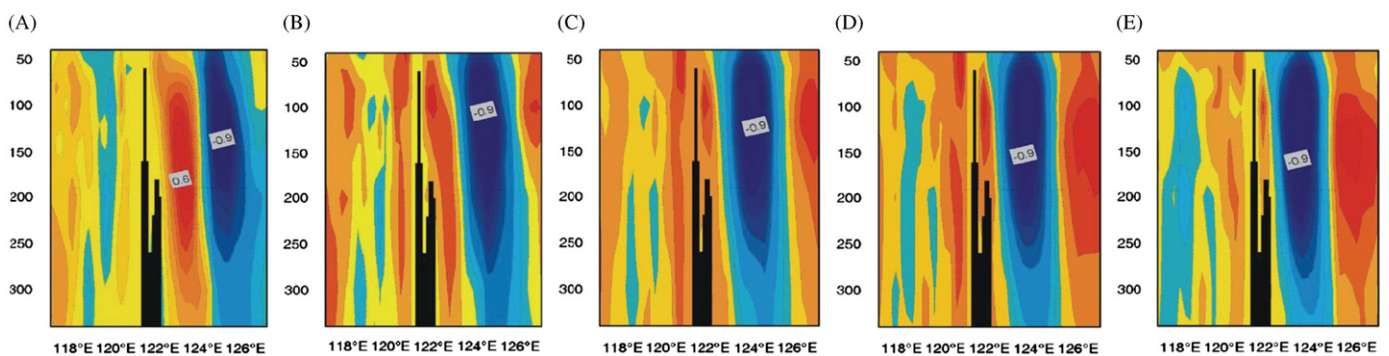

Fig. 9. Composite analysis of vertical temperature at depths from 50 m to 350 m along 19N after (A) −2 weeks (contour interval=0.1 °C), (B) −1 week, (C) 0 week, (D) 1 week, (E) 2 weeks.
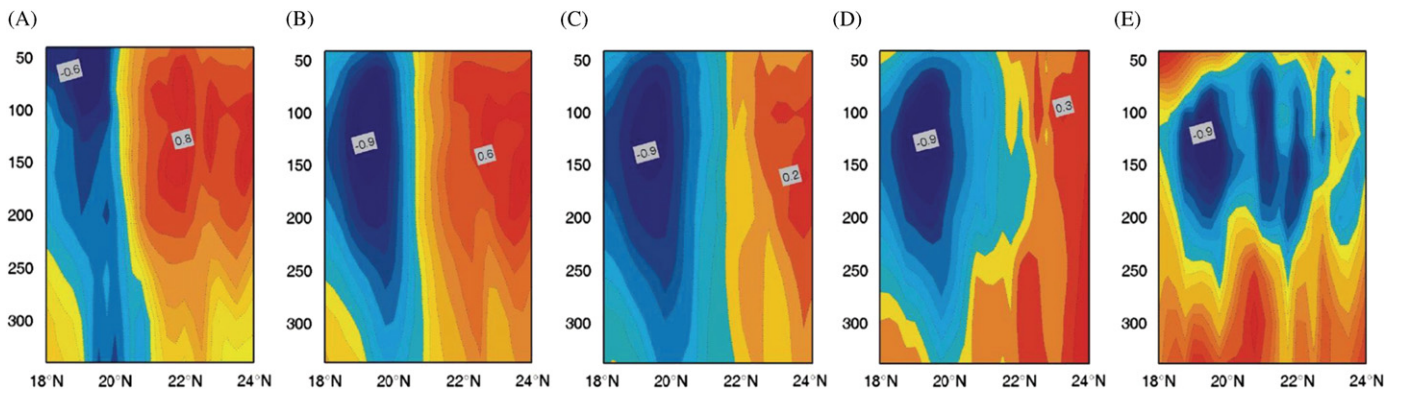
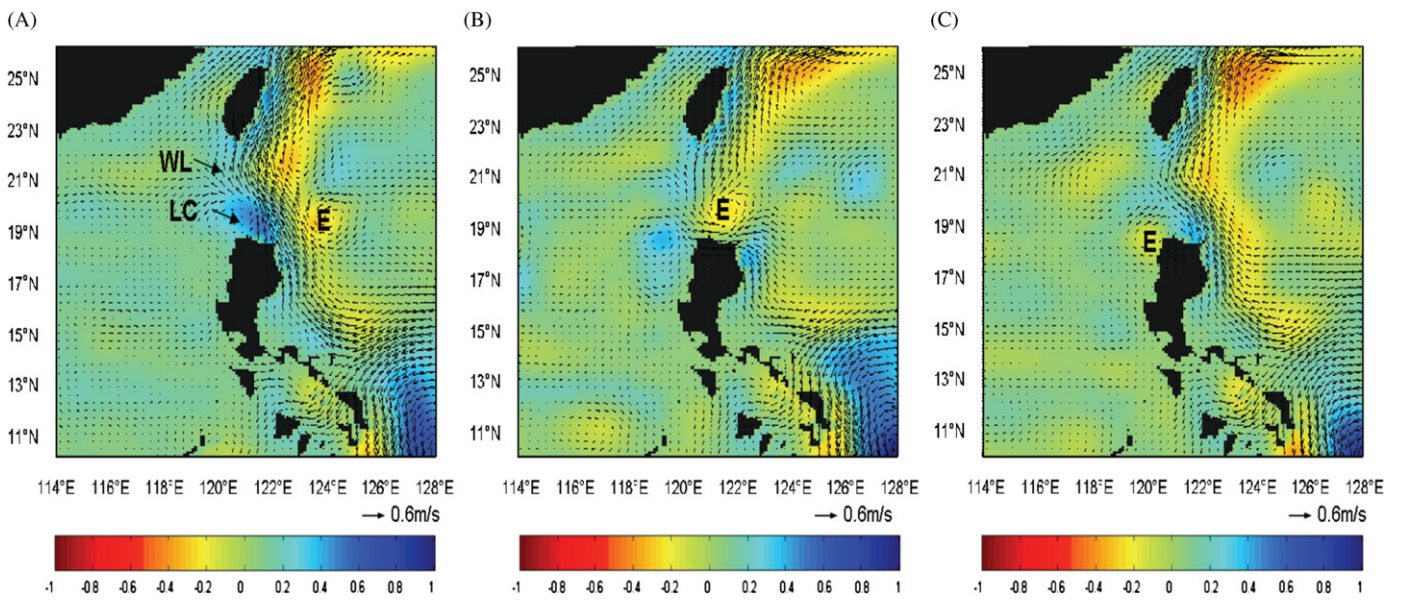**Fig. 10.** Same as Fig. 9 but along 124°E. (A) -2 weeks, (B) -1 week, (C) 0 week, (D) 1 week, (E) 2 weeks.

Fig. 11. The ensemble-averaged composites for the westward-passage pattern, $\overline{Ew}$ (Vectors show the current, and the color shading represents the vorticity, unit : 10^{-5}/s). (A) 0 Month, (B) 1 Month, and (C) 2 Months.
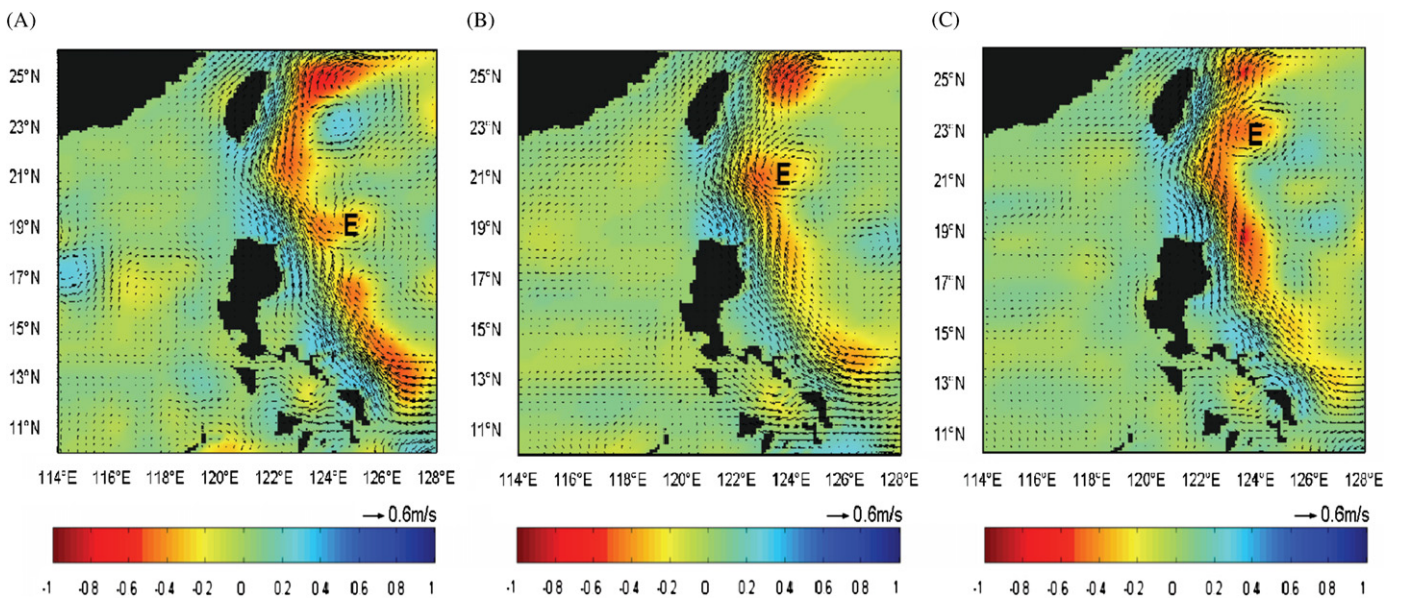

Fig. 12. Same as the Fig. 11 but for the blocking pattern, $\overline{En}$. (A) 0 week, (B) 2 weeks, and (C) 4 weeks.

looping scenario of the modeled Kuroshio. The concomitant existence of the cyclone and a westward looping of the Kuroshio is consistent with the conservation of potential vorticity. In order to conserve potential vorticity, a fluid parcel shoved northward in the western boundary current gains negative relative vorticity, which must be removed in order for the parcel to rejoin (at higher latitudes) the interior flow of negligible relative vorticity; the removal may be through lateral diffusion in the frictional wall layer (e.g. in a Munk layer; Pedlosky, 1979). The presence of a cyclonic (positive) vorticity source also compensates for the

negative vorticity, enabling the parcel to drift westward along the planetary beta-contours once it is no longer constrained by the Luzon coast, i.e. once the Kuroshio enters the Luzon Strait. That the Kuroshio tends to loop westward is clear from Fig. 11 (see also below Fig. 14). The sequential snapshots in Fig. 11 shows that a warm-core eddy originally centered at 124°E, 19°N (Fig. 11A) propagates westward. The eddy interacts with the Kuroshio (Fig. 11B) and then enters the Luzon Strait (Fig. 11C) when the westward-propagating eddy reaches the northwestern Luzon Island near 121°E, 18.5°N. The eddy-Kuroshio interaction follows closely the scenario summarized previously in Section 3 (see Fig. 2D).

Fig. 12A, B, C show the eddy-blocking or northward-propagating composite patterns ($\overline{En}$) during the time of analysis and in the following two and four weeks after an eddy interacts with the Kuroshio near 123°E, 23°N. Two weeks instead of one month (for Fig. 11) are chosen because northward-propagating eddies have approximately doubled the speed of westward-propagating eddies. Fig. 12A shows a warm-core eddy centered at 124°E, 19°N, and the Kuroshio flows northward along a relatively straight path from east of Luzon to Taiwan. In other words, the Kuroshio "leaps" across the Luzon Strait. As mentioned above, the Kuroshio in this case is highly inertial with strong transport. In contrast to the westward-passage pattern (Fig. 11A), the vorticity off the northern coast of Luzon is much weaker, $\approx 0.15 \times 10^{-5}/s$ (Fig. 12A). Conservation of potential vorticity suggests then the Kuroshio is less likely to loop into the South China Sea.

Finally, it is necessary to compare also the "PV-jump" across the Kuroshio during the blocking (the $\overline{En}$-pattern, spring-summer) and westward passage (the $\overline{Ew}$-pattern, fall-winter) modes of the eddies. Fig. 14 shows a plot at $z = -65$ m of the Ertel PV (Pedlosky, 1979) computed for the two modes. It is clear that the PV-jump during the blocking mode (Fig. 14A) is larger than that during the looping mode. It is also clear from the corresponding (u,v) vectors that the blocking (westward-passage) mode corresponds to the leaping (looping) mode of the Kuroshio. These results are again consistent with the ideas put forth in Section 3 (Fig. 2).
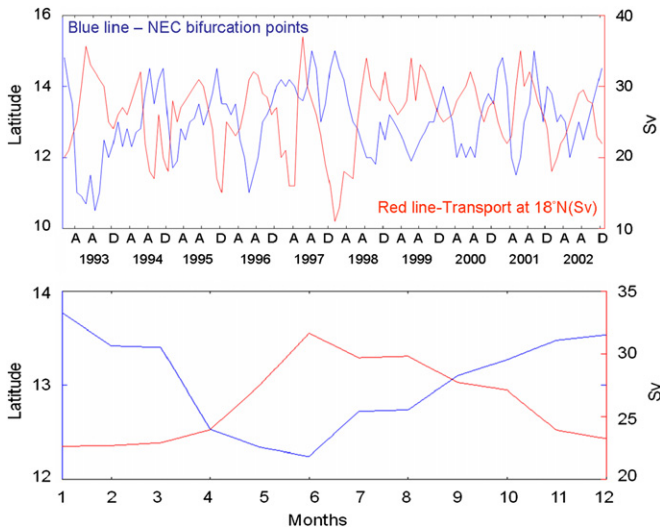

Fig. 13. Upper panel: 10-year time-series of modeled NEC bifurcation latitude (blue) and Kuroshio transport (in the upper 500 m, sigma-theta ≈ 26.5) from Luzon east coast to 125°E at 18°N (red); lower panel: monthly averages of the 10-year series. (For interpretation of the references to colour in this figure legend, the reader is referred to the web version of this article.)
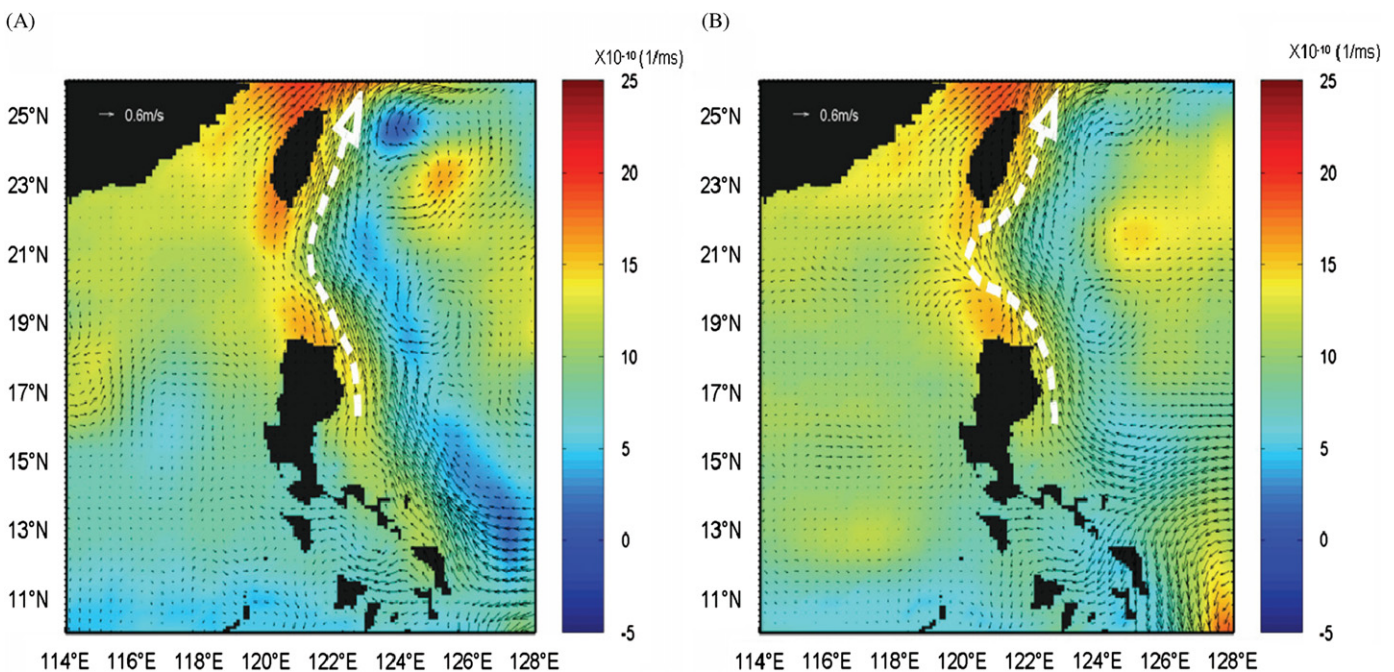

Fig. 14. Color maps of the Ertel potential vorticity at $z = -65$ m averaged over (A) the blocking and (B) westward passage modes of eddies in the Luzon Strait. The (u,v) vectors are also superimposed, and the white dashed lines sketch the Kuroshio paths showing the current's leaping mode in (A) and looping mode in (B).

6. Summary and Discussion

This study uses model results of the western Pacific Ocean to examine how westward-propagating eddies behave as they interact with the Kuroshio east of the Luzon Strait. We are particularly interested in the conditions that determine whether or not eddies can westward through the Strait into the South China Sea. Apart from being an interesting geophysical fluid dynamical problem, whether or not eddies can intrude into the South China Sea also impacts the regional circulation and mass (and nutrient) balances.

There are two types of behaviors when eddies approach the Kuroshio. The eddy either crosses the current and continues westward into the South China Sea – the westward-passage mode, or it is blocked and advected northward by the Kuroshio – the blocking mode. Whether or not an eddy can pass westward through the Luzon Strait depends on (i) the strength of transport of the Kuroshio and the PV-jump across it; and (ii) the curvature of the Kuroshio just north of the Luzon Island – i.e. on the strength of the cyclonic eddy north of the Island. Strong transports in spring-summer tend to produce a 'leaping' Kuroshio directly from Luzon to Taiwan. The PV-jump across the Kuroshio is correspondingly large, eddies are blocked and tend to drift northward along the eastern flank of the strong current. Weaker transports in fall-winter tend to produce a westward 'looping' Kuroshio into the South China Sea. The PV-jump is weak and eddies are then able to cross the Kuroshio and propagate westward through the Strait. Composite analyses also show that the blocking mode appears in spring-summer when the NEC shifts southward, while the westward-passage mode appears in fall-winter when the NEC shifts northward.

We have not addressed the source of the cyclonic eddy north of the Luzon Island (Fig. 11A). The cyclone may be a localized response of the looping Kuroshio interacting with the Luzon Island. The cyclonic vorticity may also be caused by northward advection of positive potential vorticity from a source upstream (of the Kuroshio) off the southeastern coast of the Luzon Island in the equatorial Pacific, where winter monsoon produces localized upwelling in the so called Mindanao Dome (c.f. Masumoto and Yamagata, 1991); a portion of the dome may be seen near the southeastern corner of Fig. 11. These should constitute the topic of a future study.

Acknowledgments

References

Bell, G.I., 1990. Interaction between vortices and waves in a simple model of geophysical flows. Phys. Fluids A 2 (4), 575–586.

Centurioni, L.R., Niiler, P.P., Lee, D.K., 2004. Observation of inflow of Philippine Sea surface water into the South China Sea through the Luzon Strait. J. Phys. Oceanogr. 34, 113–121.

Chelton, D.B., Schlax, M.G., 1996. Global observations of oceanic Rossby waves. Science 272, 235–238.

Chelton, D.B., Schlax, M.G., Samelson, R.M., de Szoeke, R.A., 2007. Global observations of large oceanic eddies. Geophys. Res. Lett. 34, L15606, doi:10.1029/2007GL030812.

Farris, A., Wimbush, M., 1996. Wind-induced intrusion into the South China Sea. J. Oceanogr. 52, 771–784.

Ho, C.-R., Zheng, Q., Kuo, N.-J., Tsai, C.-H., Huang, N.E., 2004. Observation of the Kuroshio Intrusion region in the South China Sea from AVHRR data. Int. J. Remote Sens. 25, 4583–4591.

Horel, J.D., 1984. Complex principal component analysis: Theory and Examples. J. Climate and Applied Meteorology 23, 1660–1673.

Hsin, Y.-C., Wu, C.-R., Shaw, P.-T., 2008. Spatial and Temporal Variations of the Kuroshio East of Taiwan, 1982–2005: A numerical study. J. Geophys. Res. 113, C04002, doi:10.1029/2007JC004485.

Hwang, C., Wu, CR., Kao, R., 2004. TOPEX/Poseidon observations of mesoscale eddies over the Subtropical Countercurrent: Kinematic characteristics of an anticyclonic eddy and a cyclonic eddy. J. Geophys. Res. 109, C08013, doi:10.1029/2003JC002026.

Knutson, T.R., Weickmann, K.M., 1987. 30–60 day atmospheric oscillations: composite life cycles of convection and circulation anaomalies. Month. Wea. Rev. 115, 1407–1436.

LaCasce, J.H., Pedlosky, J., 2004. The instability of Rossby basin modes and the oceanic eddy field. J. Phys. Oceanogr. 34, 2027–2041.

Liang, W.-D., Yang, Y.J., Tang, T.Y., Chung, W.-S., 2008. Kuroshio in the Luzon Strait. J. Geophys. Res. 113, C08048, doi:10.1029/2007JC004609.

Lorenz, E.N. (1956), Empirical orthogonal functions and statistical weather prediction, Rep. 1 Statist, Forecasting project., MIT.

Masumoto, Y., Yamagata, T., 1991. Response of the western tropical Pacific to the Asian winter monsoon: The generation of the Mindanao Dome. J. Phys. Oceanogr. 21, 1386–1398.

Mellor, G.L. (2004), User's guide for a three-dimensional, primitive equation, numerical ocean model. Rep., Program in Atmospheric and Oceanic Science, Princeton University.

Mellor, G.L., Yamada, T., 1974. A hierarchy of turbulence closure models for planetary boundary layers. Journal of Atmospheric Science 31, 1791–1806.

Mellor, G.L., Yamada, T., 1982. Development of a turbulence closure model for geophysical fluid problems. Review of Geophysics and Space Physics 20, 851–875.

Pedlosky, J.P., 1979. Geophysical Fluid Dynamics. Springer-Verlag 624pp.

Qu, T., Lukas, R., 2003. The Bifurcation of the North Equatorial Current in the Pacific. J. Phys. Oceanogr. 33, 5–18.

Roemmich, D., Gilson, J., 2001. Eddy transport of heat and thermocline waters in the North Pacific: A key to interannual/decadal climate variability? J. Phys. Oceanogr. 31 (675–687) 2001.

Shaw, P.-T., 1991. The seasonal variation of the intrusion of the Philippine Sea water into the South China Sea. J. Geophys. Res. 96, 821–827.

Sheremet, V.A., 2001. Hysteresis of a western boundary current leaping across a gap. J. Phys. Oceanogr. 31, 1247–1259.

Sheremet, V.A., Kuehl., J., 2007. Gap leaping western boundary current in a circular tank model. J. Phys. Oceanogr. 37, 1488–1495.

Smagorinsky, J., 1963. General circulation experiments with the primitive equations. I. The basic experiment. Month. Wea. Rev. 91, 99–164.

Stern, M.E., Flierl, G.R., 1987. On the interaction of a vortex with a shear flow. J. Phys. Res 92 (C10), 10733–10744.

Tseng, C.-M., Wong, G.T.F., Lin, I.-I., Wu, C.-R., Liu, K.-K., 2005. A unique seasonal pattern in phytoplankton biomass in low-latitude waters in the South China Sea. Geophys. Res. Lett. 32, L08608, doi:10.1029/2004GL022111.

Vandermeirsch, F.O., Carton, X.J., Morel, Y.G., 2003a. Interaction between an eddy and a zonal jet Part I. One-and-a-half-layer model. Dyn. Atmos. Ocean 36, 247–270.

Vandermeirsch, F.O., Carton, X.J., Morel, Y.G., 2003b. Interaction between an eddy and a zonal jet Part II. Two-and-a-half-layer model. Dyn. Atmos. Ocean 36, 271–296.

Wang, Q.-Y., Hu, D.-X., 2006. Bifurcation of the North Equatorial Current derived from altimetry in the Pacific Ocean. J. Hydrodynamics 18, 620–626.

Wu, C.-R., Hsin, Y.-C., 2005. Volume transport through the Taiwan Strait: a numerical study. Terrestrial, Atmospheric and Oceanic Sciences 16 (2), 377–391.

Wu, C.-R., Chiang, T.-L., 2007. Mesoscale eddies in the northern South China Sea. Deep Sea Res. II 54, 1575–1588.

Yang, Y., Liu, C.T., Hu, J.H., Koga, M., 1999. Taiwan current (Kuroshio) and impinging eddies. J. Oceanogr. 55, 609–617.

Yuan, D., Han, W., Hu, D., 2006. Surface Kuroshio path in the Luzon Strait area derived from satellite remote sensing data. J. Geophys. Res. 111, C11007, doi:10.1029/2005JC003412.

Zhang, D., Lee., T.N., Johns, W.E., et al., 2001. The Kuroshio east of Taiwan: Modes of variability and relationship to interior mesoscale eddies. J. Phys. Oceanogr. 31, 1054–1074.